The influence of temperature on hydrogen environmentally assisted cracking of AA7449-T7651 in moist air

Unai De Francisco, Nicolas O. Larrosa, Matthew J. Peel

Department of Mechanical Engineering, University of Bristol, UK

Abstract

The 7xxx series of aluminium alloys are sensitive to intergranular hydrogen environmentally assisted cracking (HEAC) in moist air environments. A new generation of 7xxx alloys used in aircraft components (including AA7449) have been found to be more sensitive to HEAC. This investigation aims to quantify the HEAC crack growth rates of AA7449-T7651 in moist air at different temperatures. Double cantilever beam specimens were loaded at a constant displacement and placed in moist air (80-85% relative humidity) at temperatures between 25-80°C. Regular measurements of crack length permitted the determination of the crack growth rate as a function of the stress intensity factor (K_I) during stage I (high K_I dependence of growth rate) and stage II (low K_I dependence of growth rate). Increasing the temperature was found to increase the crack growth rate during stage II cracking, following Arrhenius kinetics. The activation energy for the stage II crack growth rate at a stress intensity factor of 14.5 MPa $\sqrt{\text{m}}$ was estimated as 84.7 kJ/mol. Additionally, the threshold stress intensity factor for HEAC was found to decrease with increasing temperature. This was attributed to a higher hydrogen solubility at higher temperatures. The crack growth rate of AA7449-T7651 at room temperature was similar to that of overaged AA7050 and AA7075-T7651, ranging between 1.3-2.1×10^{-7} mm/s. It was inferred that the alloy temper has more influence than the composition during stage II cracking at room temperature.

Keywords: Fracture Mechanics, AA7449, Hydrogen environmentally assisted cracking, Double Cantilever Beam, Moist air, Aluminium Alloys

1. Introduction

Aluminium alloys of the 7xxx series have long been known to exhibit hydrogen environmentally assisted cracking (HEAC) in both moist environments and aqueous solutions, but this has generally not been of significant consequence due to the relatively slow rates of cracking under practical conditions. However, the European Aviation Safety Agency (EASA) recently reported much higher rates of cracking in components made of newer 7xxx alloys as a result of HEAC in moist air [1]. The increased sensitivity to HEAC of the alloys reported was linked to the composition, namely, a high Zn/Mg ratio and a low Cu content.

A previous investigation compared the sensitivity of AA7449-T7651 (high Zn/Mg) and AA7075-T651 (low Zn/Mg) in smooth 4-point bend samples [2]. The samples were statically loaded at different stresses below yield and held in a warm moist environment (80°C, 85% relative humidity). The high temperature was used to accelerate the formation and growth of cracks, to enable the experiment to occur within an accessible timescale. The 4-point bend tests revealed that both alloys were susceptible to the formation of macroscopic cracks. However, AA7449 was found to be sensitive at lower stress levels (as low as 40% of yield) and to form macroscopic cracks much more rapidly. This study was useful in comparing the kinetics of crack formation and the microstructural crack growth behaviour of both alloys. However, the high temperature at which the tests were performed does not allow for an accurate prognosis of the formation of cracks in aircraft components, which are typically exposed to much lower temperatures. Additionally, these tests were focused on population level crack analysis and less suited to providing quantitative crack growth rates of single cracks under controlled conditions.

The measurement of crack growth rates under HEAC

Email address: ud13050@bristol.ac.uk (Unai De Francisco)

conditions, in a wide range of 7xxx alloys, has frequently been assessed using statically loaded fracture mechanics samples in different environments [3, 4, 5, 6, 7, 8]. Typically, fracture mechanics tests are performed using double cantilever beam (DCB) samples. These are suitable for testing the short transverse direction of high strength aluminium alloys, as HEAC is intergranular and the sample geometry prevents the crack from running out of plane. From these tests, the crack growth rate (v) dependence on the stress intensity factor (K_I) can be determined, providing a practical method to compare the sensitivity of alloys in different environments. The v vs K_I curves during HEAC typically present two different regimes: i) *stage I* - at low K_I the crack growth rates increase significantly with increasing stress intensity factor; ii) *stage II* - at higher K_I the crack growth rate shows little dependence on the stress intensity factor. In many cases the crack growth rate during stage II is completely K_I-independent and shows as a plateau in the v vs K_I curve [3].

Despite the importance of the alloys reported by the EASA (including AA7449), there is little available fracture mechanics HEAC data in the public domain. This data is indispensable for aircraft design in order to adapt the material behaviour to the requirements of the maintenance concepts and to ensure that defined inspection intervals are adhered to [9]. Further, its absence prevents quantitative comparisons of the sensitivity with other 7xxx alloys. Schwarzenböck et al investigated several new generation alloys, including 7449, using DCB samples at 70°C and compared their cracking rates to the older 7050 alloy [10]. Although restricted to the study of one temperature, they demonstrated that all the new alloys displayed increased crack growth in both stage I and stage II along with a lower threshold in stress intensity to initiate growth. Young and Scully investigated the effect of temperature on the HEAC crack growth rates of AA7050 and a 7xxx alloy with low Cu content at different temperatures in moist air [5]. The study revealed that the stage II crack growth rates increased exponentially with temperature, according to the Arrhenius equation. However, there is no available data on the influence of temperature on the stage I crack growth rates during HEAC in moist air. The lifetime of aircraft components is dominated by the stage I behaviour, as the crack growth rates are much lower for small cracks and defects. Therefore it is of interest to investigate the crack growth rates at a low stress intensity factor range. This allows to better approximate the lifetime of components at the design stage. Further, a threshold stress intensity factor, K_{IEAC}, can be approximated. This parameter represents a stress intensity factor below which cracking is deemed negligible.

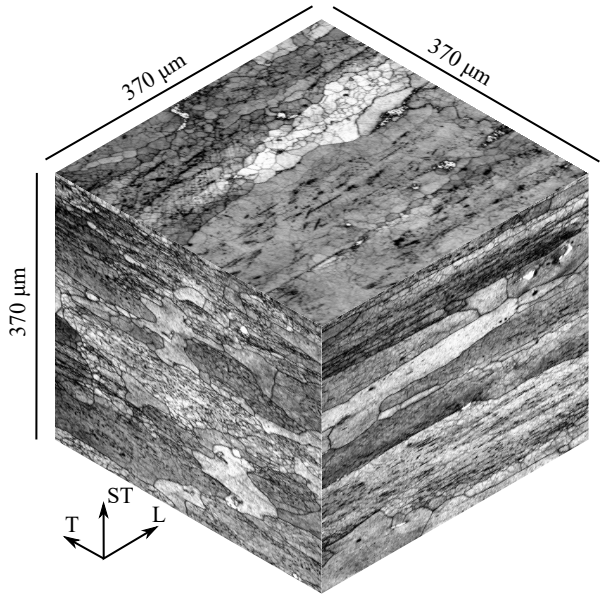

Figure 1: The etched microstructure of AA7449-T7651 along three different planes. Etching was performed by immersion in Weck's reagent during 15 seconds.

This article describes the use of DCB specimens for the analysis of HEAC of the novel AA7449-T7651 in moist air. The purpose of this study is twofold: (a) to determine the macroscopic crack growth rates of AA7449-T7651 during HEAC in moist air and (b) to analyse the effect of temperature on the crack growth rates during stage I and stage II.

2. Experimental Methods

2.1. Material and sample preparation

The material used in this study was AA7449-T7651 (Table 1) obtained as a rolled 80 mm thick plate. The T7651 temper is achieved by solution heat treating, stress relieving by stretching and artificially ageing to an overaged condition. The microstructure of the alloy is illustrated in Figure 1, where L, T, and ST stand for the longitudinal, transverse and short transverse axes respectively.

Figure 2 shows the dimensions of the DCB specimens used for the experiments (from ASTM Standard G168-17 [12]). The samples were cut in the ST-T orientation (axes included in Figure 2) at the mid-plane (T/2) by electrical discharge machining (EDM). Subsequently the outer faces were ground using 600 grit SiC paper, in order to remove the EDM-affected layer and allow for the visibility of cracks. The samples were rinsed with

Table 1: Composition of AA7449 given in weight percent maximum unless shown as range. The compositions of alloys used for DCB tests in other studies have also been included below for comparison (AA7449, AA7050 and AA7075).

Alloy [Ref.]	Zn	Mg	**Cu**	Fe	Si	Mn	Zr+Ti	Zr	Ti	Cr	**Zn/Mg**
AA7449 [11]	7.5-8.7	1.8-2.7	1.4-2.1	0.15	0.12	0.2	0.25	-	-	-	2.8-4.8
AA7449 [10]	8.4	2.1	1.9	0.08	0.03	-	-	0.11	-	-	4.0
AA7050 [5]	6.09	2.14	2.19	0.09	0.05	-	-	0.11	-	-	2.9
AA7075 [11]	5.1-6.1	2.1-2.9	1.2-2.0	0.5	0.4	0.3	-	-	0.2	0.18-0.28	1.8-2.9

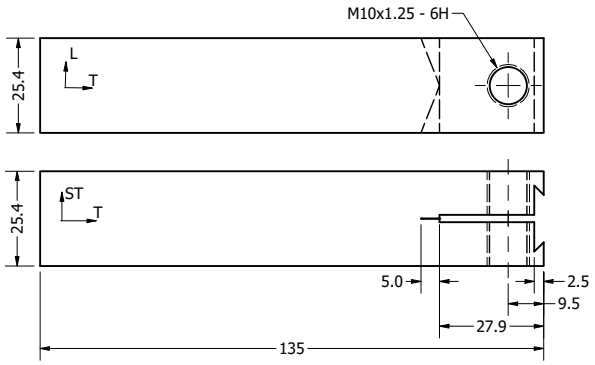

Figure 2: Drawing of the DCB specimens. Dimensions in mm.

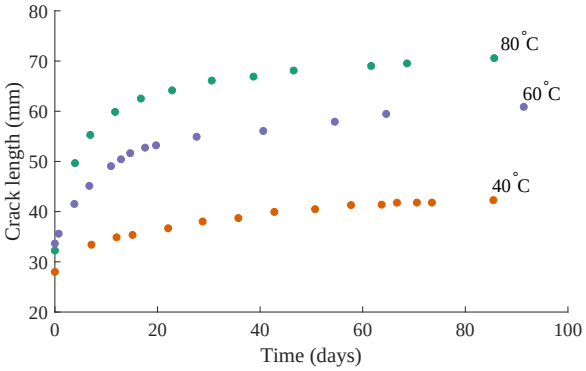

Figure 3: Graph showing the crack length evolution with time of DCB samples of AA7449-T7651 exposed to moist air at different temperatures.

acetone and blow dried immediately after grinding. The samples were then stored in a desiccator with silica gel for at least one week prior to loading.

2.2. Loading and environmental exposure

The ASTM standard procedure G168-17 was followed to estimate the v vs K_I curves from the DCB specimens [12]. The samples were fatigue precracked in laboratory air. Subsequently the samples were held at a constant crack mouth opening displacement (CMOD) by two M10 stainless steel bolts. The CMOD was monitored using a clip on Instron® COD gauge during loading. Once loaded, the samples were exposed to the required moist environment. At regular intervals, the samples were removed from the moist environment and imaged on both sides using an optical microscope to measure the crack length. The samples were removed from the environment by opening the oven/environmental chamber and handling them with nitrile gloves. Condensation was not an issue during removal, as the samples were warmer than the laboratory air. The samples were placed on the microscope quickly after removing them from the ovens, and placed using a custom-made stand to avoid contaminating or damaging the sample. The crack length was measured from the microscope images by recording the distance from the loading axis to the crack tip. The crack length was calculated as an average of both sides. Therefore, the actual crack length due to tunnelling was not considered. Figure 3 presents the crack length of three DCB samples of AA7449-T7651 exposed to moist air at different temperatures. Finally, v and K_I were estimated from the average crack lengths and the exposure time [12]. The measurement time of the samples was approximately 30 minutes. Afterwards, the samples were reintroduced into their respective moist environments. It is important to prevent the condensation of water when introducing the DCB samples into the warm, moist environments. Therefore, the samples were preheated to the exposure temperature using an electronically-controlled oven prior to being placed in the moist environment. Once heated, the samples were carefully introduced into the corresponding humidity chamber/container, operating at the required conditions.

The samples were exposed to moist air at temperatures (T) of 25°C, 40°C, 60°C and 80°C. The samples at 80°C were exposed to moist air using a Vötsch electronically controlled chamber set to a relative humidity (RH) of 85%. For all other temperatures, a constant relative humidity was maintained by placing the samples inside a sealed container with a KCl saturated salt solution (not in contact with sample), following the pro-

Table 2: Description of the DCB samples displayed in Figure 4. The samples of AA7449-T7651 correspond to the experiments performed in this investigation, with the exception of data at 70°C, obtained by Schwarzenböck et al. [10]. The method of exposing the samples to a moist environment is specified in the first column, where possible.
Elec.: environment controlled by electronic chamber.
Salt sol.: environment using the method outlined by the ASTM standard E104-02 [13].

Exposure type	Alloy [Ref.]	T (°C)	RH (%)	V_0 (mm)
Elec.	7449-T7651	80	85	0.9
Elec.		80	85	1.0
Salt sol.		60	80	1.0
Salt sol.		40	82.3	0.8
Salt sol.		40	82.3	1.0
Salt sol.		25	84.2	1.0
Elec.	7449-T7651 [10]	70	85	-
Elec.	OA 7050 [5]	60	90	-
Elec.		40	90	-
Elec.		25	90	-
-	7075-T7651 [3]	23	100	-
-	7075-T651 [3]	23	100	-

cedure of the ASTM standard E104-02 [13]. The desired temperature was achieved by placing the sealed container with the sample and KCl solution inside an electronically-controlled oven. The humidity was not independently monitored for every container with saturated KCl solutions. However, previous tests were used to verify that the steady state relative humidity matched the quoted values in the ASTM standard E104-02.

In total, six samples were tested. The steady state environmental conditions and the crack mouth opening displacement (V_0) to which the samples of AA7449-T7651 were subjected are summarised in Table 2. Repeat samples were used at 40 and 80°C to identify possible systematic errors and analyse the scatter between different samples.

2.3. Chloride gas during experiment

The DCB samples of AA7449 for temperatures ranging between 25-60°C were exposed to moist air using saturated KCl solutions [13]. It has been identified that the use of NaCl and KCl solutions results in the presence of HCl gas in the environment [14]. The effect of the HCl gas concentration on HEAC of 7xxx alloys has not been investigated. However, the presence of halide ions in aqueous solutions is known to increase the crack growth rate during stage II [3]. Therefore, the presence of HCl gas may enhance cracking during DCB tests.

Table 3: Partial pressure of HCl (g) and H_2O (g) in the environment using saturated KCl solutions.

T (°C)	P_{HCl} (Pa)	P_{H_2O} (kPa)	P_{HCl}/P_{H2O} (%)
25	6	2.39	0.26
40	38	5.20	0.73
60	346	14.68	2.36

The partial pressure of hydrochloric acid gas increases exponentially with temperature in the same way as the partial pressure of water vapour when using salt solutions [15]. Using the solubility curve of KCl, the molality of the saturated KCl solutions was estimated at the different temperatures [16]. By using the molality, the partial pressures of water vapour (P_{H_2O}) and HCl gas (P_{HCL}) at different temperatures were extrapolated from the data by Fritz et al. [15]. These are presented in Table 3. The ratio of P_{HCL}/P_{H_2O} is low at 25° and 40°C of approximately 0.26 and 0.73% respectively. Therefore the influence of HCl gas can be considered negligible at low temperatures. However, at 60°C the ratio is 2.36% and the effect of HCl gas may be more significant. Further research will focus on the effect of the gaseous HCl content on the crack growth rates of 7xxx alloys to ascertain the validity of the method.

2.4. Microscopy

Optical microscopy and etching were performed to image the cracks relative to the microstructure. Etching was performed on the exterior surface of the samples (T-ST plane). The polished surfaces were etched by immersion in Weck's reagent for 20 seconds. Additionally, scanning electron microscopy (SEM) was used to visualise the HEAC fracture surfaces. This was done using a Hitachi TM3030 plus SEM machine, operating at 15kV. Imaging was performed using back-scattered electrons to enhance the contrast between the aluminium matrix and other intermetallic phases.

3. Results

3.1. Crack growth rate

The variation in crack growth rate as a function of K_I for all six samples of AA7449-T7651 (at 25, 40, 60 and 80°C) tested are shown in Figure 4. The crack growth rates in moist air environments of other alloys have also been included in the graph for comparison. This data corresponds to: (a) stage I and II cracking of

AA7449-T7651 at 70°C [10], (b) stage II cracking at various temperatures of overaged (OA) AA7050 [5] and (c) stage II cracking at room temperature of AA7075 in the -T651 and -T7651 tempers [3]. It must be noted that the tests for [5] and [3] were performed at a relative humidity of 90% and 100% respectively. In these cases, small changes in temperature can lead to condensation. Therefore, these samples might be sensitive to stronger micro-galvanic corrosion, which can in turn enhance the crack growth rates. However, this seems unlikely in the case of [5], as the DCB specimens were only subjected to a single exposure to moist air. The composition of AA7449, AA7050 and AA7075 in these investigations have also been included in Table 1. The environmental conditions at which the other tests were performed have also been included in Table 2. The crack growth rates for AA7050 obtained by Young and Scully were determined exclusively for stage II cracking [5]. This was done by examining the crack growth experienced during a single exposure. The crack growth was found to be completely constant during this plateau stage. Therefore, this data is presented in Figure 4 by showing the initial and final stress intensity factor at the recorded crack growth rate.

Only two data points were collected for the sample of AA7449-T7651 exposed to moist air at room temperature, as no noticeable cracking was observed after subsequent extended exposure. Therefore, it is unclear where the data points lie relative to the stage II plateau. Several observations can be made from Figure 4:

1. The stage II crack growth rates at room temperature of the overaged alloys (7075-T7651 and OA 7050) were very similar to the crack growth rates of AA7449-T7651, ranging between 1.3-2.1×10^{-7} mm/s.
2. The peak aged alloy 7075-T651 shows a much larger stage II crack growth rate of 5.1×10^{-6} mm/s at room temperature.
3. The stage I and II crack growth rates of AA7449-T7651 increase significantly with temperature and a shift can be seen towards lower values of K_I, indicating a lower K_{IEAC}.
4. The crack growth rates of AA7449-T7651 collected in this study are in good agreement with those at 70°C, obtained by Schwarzenböck et al. [10]. However, the data points at 70°C are closer to those at 60°C than at 80°C. This may be associated to the HCl gas content present when using salt solutions to maintain a constant relative humidity.

In Figure 4, stage I and II cracking of AA7449-T7651 have been labelled as I and II respectively. It can be seen that in both stages, the crack growth rate increases exponentially with K_I. This has been shown by fitting linear regression lines in the semi-log graph (dashed for stage I and dash-dot for stage II). It is clear from the gradient of the regression lines that the stress intensity factor dependence is much greater during stage I. In contrast to AA7449, the data of AA7050 during stage II shows a completely K_I independent crack growth rate even at temperatures of 40°C and 60°C.

Table 4: Table showing the approximate stress intensity factor at the onset of Stage II and Stage I (approximated as K_I where v = 1.3×10^{-7} mm/s) at different temperatures for AA7449-T7651.

T (°C)	25	40	60	80
Stage I onset (MPa $\sqrt{\text{m}}$)	16.7	12.2	-	5.6
Stage II onset (MPa $\sqrt{\text{m}}$)	-	12.9	9.5	8.3

Figure 4 shows that AA7449-T7651 becomes more sensitive to HEAC with increasing temperature. In order to obtain an estimate of the environmentally assisted cracking threshold stress intensity factor, K_{IEAC}, the ASTM standard E1681-03 recommends that that the test duration should be greater than 10,000 hours for aluminium alloys at constant displacements. Therefore, this value cannot be estimated accurately from the present data. However, estimates for the stress intensity factor at which the crack growth rate drops below 1.3×10^{-7} mm/s can be obtained from Figure 4 and are shown in Table 4. It can be inferred that K_{IEAC} decreases notably as the temperature increases. Table 4 also shows the approximate value of K_I above which stage II cracking was identified at different temperatures. It can be seen that the onset of stage II cracking also occurs at lower values of K_I with increasing temperature.

3.2. Activation energy analysis

In order to analyse the influence of temperature on the HEAC crack growth rates, it is useful to perform an activation energy analysis using the Arrhenius equation. This equation is useful as the crack growth rates are typically found to increase exponentially with temperature. The resulting activation energy can be used as a measure of the sensitivity of HEAC of the alloy to changes in temperature. The Arrhenius equation for the stage I and II crack growth rates (v_I and v_{II}) should be performed independently. v_I and v_{II}, can be expressed as [3]

$$v_{I/II} = v_0 \exp\left[(cK_I - Q_{eff})/RT\right], \quad (1)$$

where v_0 is the pre-exponential factor, c and Q_{eff} are experimental constants and R is the ideal gas constant.

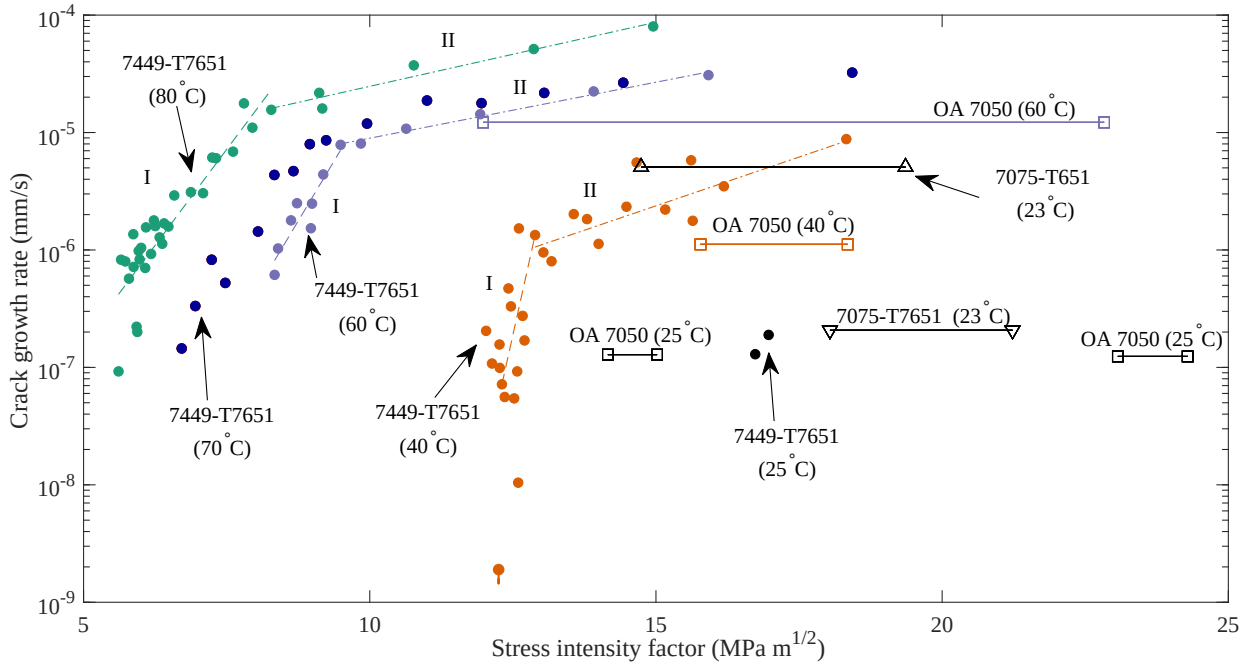

Figure 4: Semi-log graph showing the crack growth rate as a function of K_I for samples of AA7449-T7651 loaded at different temperatures (solid dots). Stages I and II have been labelled as I and II respectively. Data from other sources have been included for comparison. The additional data includes: (a) stage I and II crack growth rates of AA7449-T7651 exposed to moist air at 70°C [10], (b) stage II crack growth rates of AA7050 [5] and (c) stage II crack growth rates of AA7075 [3]. The temper and environmental exposure of external experiments can be seen in Table 2).

Previous Arrhenius analyses by Young and Scully of stage II cracking of AA7050 do not contain the cK_I term ($c = 0$), as the crack growth rates showed a complete plateau [5]. In this case, the stage II crack growth rate for AA7449 was not K_I independent and the cK_I term cannot be ignored. To simplify the analysis, given that the crack growth rate was not constant during stage II, the analysis was performed for a single stress intensity factor of $K_I = 14.5$ MPa $\sqrt{\text{m}}$. Thus, the $cK_I - Q_{eff}$ terms become a constant and equation 1 can be simplified to

$$v_{II}(K_I = 14.5) = v_0 \exp\left[(-Q_{eff})/RT\right]. \quad (2)$$

A value of 14.5 MPa $\sqrt{\text{m}}$ was selected as the DCB samples subjected to temperatures ranging between 40-80°C were all in stage II at this K_I. The values of v_{II} at $K_I = 14.5$ MPa $\sqrt{\text{m}}$ for the temperatures ranging between 40-80°C were obtained by interpolating from the linear regression lines (dash-dot) in Figure 4. These values are presented in the Arrhenius plot in Figure 5, together with the Arrhenius regression line following equation 2. The resulting pre-exponential factor (y-intercept, v_0) and activation energy (gradient, $-Q_{eff}$) from Figure 5 are presented and compared to those of peak aged (PA) AA7050 and OA AA7050 obtained in [5] in Table 5. It can be seen that both experimental constants for AA7449-T7651 are similar to those of AA7050 in the peak aged condition. However, the uncertainty in the activation energy was very large, estimated as ±29 kJ/mol. This can be associated to the large variance in the interpolation of the stage II crack growth rate for the samples subjected to 40°C.

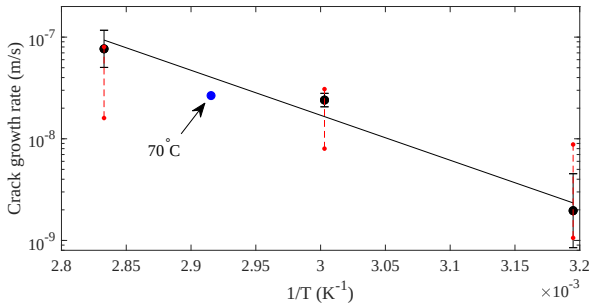

Figure 5: Arrhenius plot of the stage II crack growth rate of AA7449-T7651 corresponding to $K_I = 14.5$ MPa $\sqrt{\text{m}}$. Error bars show the 95% confidence interval of the crack growth rates interpolated from the fits in Figure 4. A red dashed line has been included to show the range of v_{II} values recorded at each temperature. The data point at 70°C corresponding to AA7449-T7651 [10] has been included for comparison.

Since the Arrhenius analysis was performed for a single stress intensity factor, it does not account for

Table 5: Comparison of the pre-exponential factor and activation energy of AA7449-T7651 (at K_I = 14.5 MPa $\sqrt{\text{m}}$) and AA7050 in a PA and OA condition. The uncertainty for $-Q_{eff}$ is given as a 95% confidence interval, propagated from the uncertainty in the estimates of v_{II} from Figure 5.

Alloy [Ref.]	v_0 (m/s)	$-Q_{eff}$ (kJ/mol)
7449-T7651	3.20×10^5	84.7 ± 29
OA 7050 [5]	2.61×10^7	98.4
PA 7050 [5]	1.93×10^5	82.1

the complete range of v_{II} values obtained during stage II cracking. The minimum and maximum v_{II} values recorded at each temperature have been displayed with dashed red lines in Figure 5. It can be seen that the range is much greater for the samples subjected to 40°C, as the crack growth was recorded at higher stress intensity factors. Further experiments are required to ascertain whether the crack growth rates steady out to a constant value at higher levels of stress (K_I > 20MPa $\sqrt{\text{m}}$). The crack growth rate at K_I = 14.5MPa $\sqrt{\text{m}}$ for the data corresponding to 70°C [10] has been included in Figure 5 for comparison. The data point is close to the trend-line, indicating that the systematic errors from the use of KCl solutions do not undermine the Arrhenius analysis.

3.3. Crack morphology

Figure 6 shows the crack of a DCB sample of AA7449-T7651 relative to the surrounding microstructure, obtained via microscopy and etching. Figures 6(a)-(b) contain images of the crack tip, Figure 6(c) shows the crack at a region with a higher stress intensity factor, and Figure 6(d) shows a section of the fatigue pre-crack region. It is clear that the in the HEAC regions (Figures 6(a)-(c)), cracking is predominantly intergranular in comparison to the fatigue pre-crack region. This was the case at all temperatures. At the crack tip, the crack shows crack segmentation and branching, particularly in the presence of recrystallised grains (free of a visible subgrain structure). The generally smaller and more equiaxed recrystallised grains can be seen to deviate the crack from the main propagation direction (T axis). This results in the observed bifurcations and final arrest at a recrystallised grain. Similar observations were made from microscopic cracks initiating and propagating in smooth samples of AA7449; revealing the same crack propagation mechanisms relative to the microstructure [2]. In contrast, Figure 6(c) does not display any segmentation. However, at high K_I, isolated tortuous regions with transgranular growth were seen. An example has been labelled in Figure 6(c). This step can be identified to be transgranular rather than propagating along the boundaries of subgrains, as it is composed of two flat steps almost perpendicular to the crack propagation direction. Figure 7(c) shows an example of a transgranular step on the fracture surface of a sample. These regions are likely to occur due to the coalescence of crack segments approaching each other. Therefore, it is likely that crack segmentation also occurred during early cracking; but cracks coalesced after prolonged crack growth.

Figure 7 shows images of the fracture surface of the HEAC region in a sample of AA7449. Many grains were found to be lifted off from the fracture surface. An example is labelled in Figure 7(a). The grains were lifted along the longitudinal direction. The lifted grains can be attributed to crack branching, where parallel cracks propagated at both sides of the grain. Additionally, the high magnification image in Figure 7(b) clearly shows the faceted intergranular surface with the presence of constituent particles. The small ductile facets correspond to the subgrains in the microstructure. The coarse particles were identified as Mg_2Si and Al-Cu-Fe using energy dispersive spectroscopy. In addition, smaller precipitates and dispersoids were also resolved, as seen by the small white speckles in Figure 7(b). The density of these precipitates varies across the fracture surface. This may be due to varying precipitation rates at different grain boundaries or differences in the exact fracture location relative to the grain boundary. Secondary cracks at grain boundaries along the longitudinal direction were also detected, as labelled in Figure 7(b). Further, the parallel striations typically found in HEAC surfaces, and attributed to discontinuous cracking, were not detected [17]. However, this may be due to the limited resolution of the fractographs. The resolution in Figure 7(b) is approximately 0.13 μm/pixel, whereas the the spacing of the parallel striations is typically in the range of 200-500 nm [17].

4. Discussion

Crack propagation during HEAC of 7xxx alloys requires the accumulation of sufficient hydrogen at sites with a high localised triaxial stress [18]. The build-up of hydrogen allows for cracking at low tensile stresses below yield. Many different hydrogen embrittlement mechanisms have been previously formulated for the reduction in the fracture stress, including: the formation of brittle hydride phases [17, 19], hydrogen enhanced localised plasticity [20] and adsorption-induced decohesion [21]. However, it is not clear which hydrogen embrittlement mechanism is responsible for HEAC of 7xxx

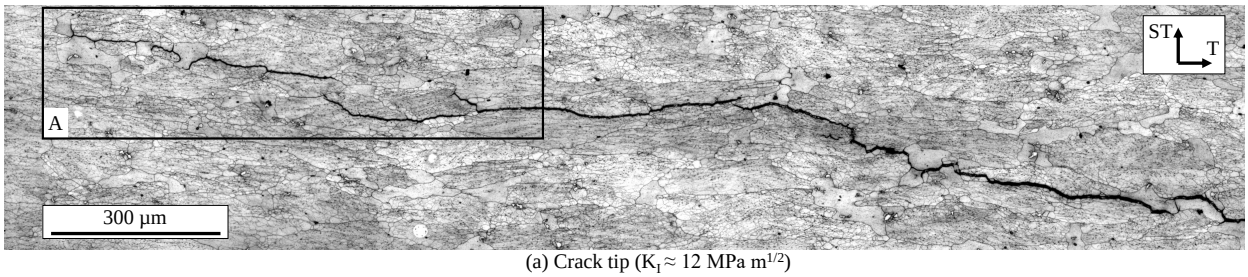

(a) Crack tip ($K_I \approx 12$ MPa $m^{1/2}$)

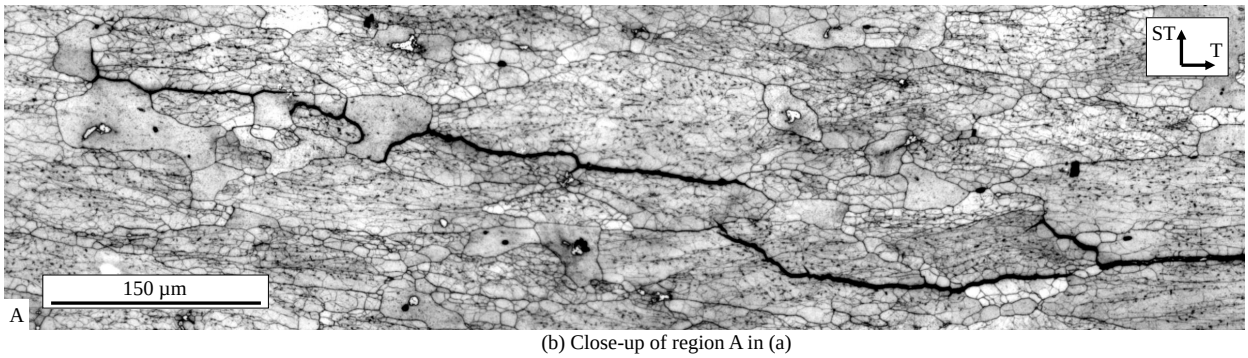

(b) Close-up of region A in (a)

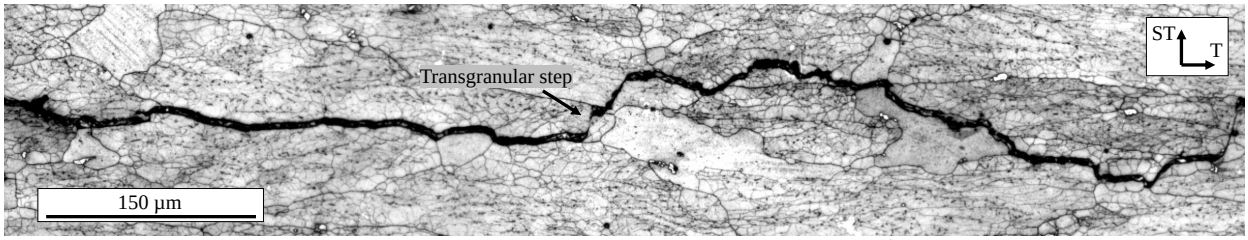

(c) Region during initial crack propagation ($K_I > 15$ MPa $m^{1/2}$)

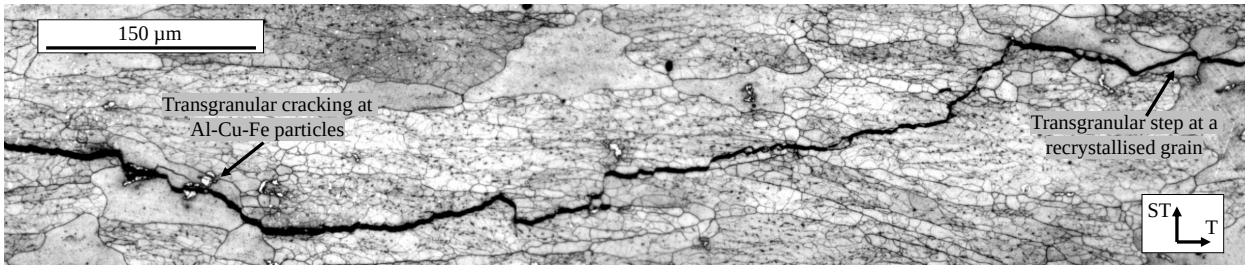

(d) Fatigue pre-cracking region

Figure 6: Micrographs showing a crack in a DCB sample of AA7449-T7651 exposed to 40°C. The sample surface was polished and etched by immersion in Weck's reagent to reveal the underlying microstructure. (a)-(b) The crack tip of the sample, where the crack can be seen to be separated into several segments. (c) A region with a higher stress intensity factor. (d) A region corresponding to fatigue pre-cracking.

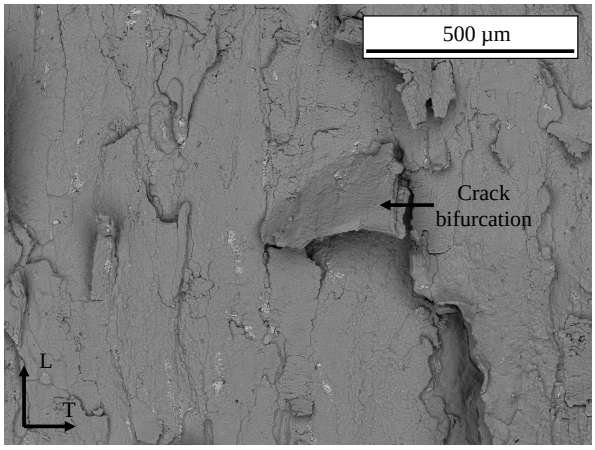

(a)

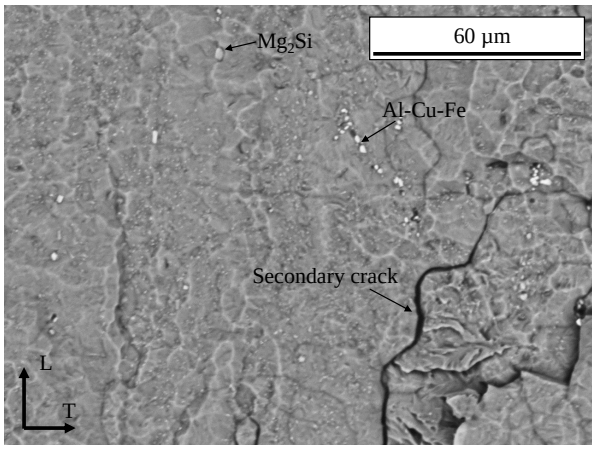

(b)

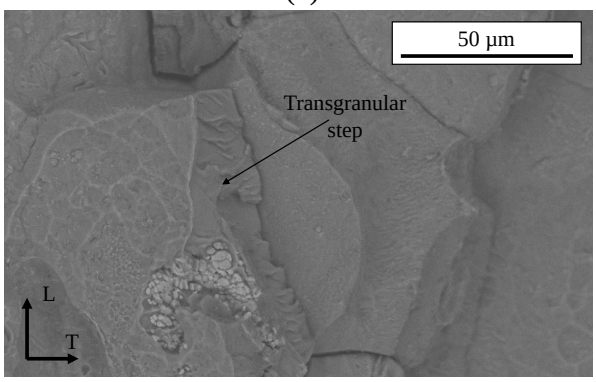

(c)

Figure 7: SEM fractographs of the HEAC region in a sample of AA7449 exposed to moist air at 80°C. Coarse particles were identified using energy dispersive spectroscopy.

alloys. The results in this investigation are insufficient to emphasise a particular hydrogen embrittlement mechanism. However, the results are useful for performing a quantitative comparison of the crack growth rates and K_{IEAC} at different temperatures. The threshold value K_{IEAC} represents an equilibrium quantity: the minimum stress intensity factor at which cracking may be identified given an unlimited amount of time. In contrast, the crack growth rates, v_I and v_{II}, are a measure of the rates at which processes during HEAC occur. This may include the hydrogen development reaction, the rate of hydrogen accumulation and/or the rate of the hydrogen embrittlement mechanism.

4.1. Effect of temperature on K_{IEAC}

Accurate values could not be determined for the threshold stress intensity factor, K_{IEAC}, because of the insufficient duration of the experiments. However, from the stage I curves, it was deduced that K_{IEAC} decreases notably with increasing temperature. This suggests that increasing the temperature not only increases crack growth rates, but also allows cracking at lower stress levels. Similar observations were made for the temperature dependence of 7xxx alloys in aqueous solutions, including distilled water, KI and NaCl solutions [3, 22].

Lee et al. found a reduction in K_{IEAC} with increasing temperature of Al-Zn-Mg alloys subjected to HEAC in saline solutions [22]. They suggested that an anodic dissolution mechanism was consistent with this decrease in K_{IEAC} with increasing temperature [22]. Therefore, since their tests were performed in aqueous solutions, it was inferred that stage I cracking occurred due to anodic dissolution at the grain boundaries. However, the present study shows that a decrease in K_{IEAC} at higher temperatures has been demonstrated to occur in moist air as well. Previous investigations show that HEAC fracture surfaces in moist air contain strengthening precipitates and Mg_2Si constituent particles [7, 17, 23], despite these being more anodic than the aluminium matrix [24]. It is therefore unlikely that an anodic dissolution mechanism is responsible for HEAC in moist air during stage I. However, the conditions for the fractographs in Figure 7 are insufficient to verify the presence of localised surface corrosion.

The local hydrogen solubility, C_s, can also be expressed using the Arrhenius equation [25]

$$C_s = C_0 \sqrt{p} \exp\left[\frac{-\Delta H_s}{RT}\right], \tag{3}$$

where C_0 is a pre-exponential constant, p is the partial pressure of the hydrogen containing gas (water

vapour) and ΔH_s is the enthalpy of solution. It follows that the decrease in K_{IEAC} with increasing temperature may be caused by an increase in the hydrogen solubility. It must be noted that enhanced plasticity at higher temperatures may result in crack blunting. Consequently, the hydrostatic stress at the fracture process zone is reduced and local hydrogen concentrations may decrease [22]. However, it is sensible to assume that the effect of crack tip blunting is negligible for a temperature range of 25-80°C. Therefore, the overall hydrogen concentration at the fracture process zone increases with temperature following equation 3. Additionally, the partial pressure of water vapour (p) increases with temperature given a constant relative humidity. This increases even further the solubility. In reality, this equation is likely to be simplistic as it does not differentiate between diffusible hydrogen (interstitial and reversibly trapped) and irreversibly trapped hydrogen [26]. Microstructural imperfections such as dislocations, precipitates and voids can act as local trap sites for absorbed atomic hydrogen [27]. Depending on the binding energy of the trap sites, they may act as irreversible trap sites which reduce the diffusivity. In turn, this can decrease the crack growth rates by delaying the accumulation of atomic hydrogen [23]. However, the role of diffusible and irreversibly trapped hydrogen on the actual hydrogen embrittlement mechanism is not well understood.

4.2. Crack growth rate

From Figure 4 it was clear that during stage II, v_{II} increased exponentially with increasing K_I for 7449-T7651. This was in contrast to the other alloys (7050 and 7075) included in the graph, which show a complete plateau. It can therefore be deduced that there may be differences in the crack growth mechanism during stage II with other alloys.

The crack growth rates for both stage I and II appeared to increase significantly with temperature. The regression line in Figure 5 indicated an acceptable fit with the Arrhenius equation for stage II cracking, despite the lack of data points. The increase in crack growth rate with temperature may be attributed to increases in the rate limiting step for hydrogen transport to the critically stressed regions. These may be the hydrogen embrittlement mechanism causing fracture, the surface reaction rates, the hydrogen diffusion rates or the rate of transport of water vapour molecules to the alloy surface [28].

The crack growth dependence on K_I is much greater during stage I. Therefore, the rate limiting step was likely to be different during stage I and stage II. From Figure 4 the stage II regression lines for AA7449-T7651 appear to have a similar gradient at different temperatures. The implication is that the Arrhenius analysis from equation 1 seems reliable, despite the small range of temperatures that were tested. In contrast, the gradient of stage I regression lines decreases with increasing temperature, showing less dependence on the stress intensity factor.

The scatter of the data during stage II was greatest for the samples of AA7449 exposed to 40°C. The samples at 60°C and 80°C showed almost no scatter. This is likely to be caused by the increased reactivity of the environment at high temperatures. Due to the greater crack growth rates at high temperature, the amount of crack growth between measurements was larger. Therefore, the statistical scatter from microstructural effects was likely to be less. Additionally, the greater scatter observed during stage I cracking may be associated to the pronounced influence of the microstructure (such as poorly oriented grain boundaries) on slowing crack growth. This can be inferred from Figure 6, where crack segmentation was more severe at the crack tip than regions with a higher stress intensity factor.

4.3. Effect of composition and ageing

The degree of ageing of the different alloy systems plotted in Figure 4 cannot be exactly quantified and compared, because microstructural features can differ strongly. However, the crack growth rates of the different alloys can be compared to speculate on the effects of composition and ageing on the crack growth rates.

At room temperature, the overaged alloys AA7075-T7651 and OA AA7050 have very similar crack growth rates relative to AA7449-T7651, ranging between 1.3×10^{-7} and 2.1×10^{-7} mm/s. However, the Zn/Mg ratios (Table 1) of the alloys differ considerably. The order of the alloys by decreasing Zn/Mg ratio is the following 7449(2.8-4.8)>7050(2.9)>7075(1.8-2.9). Therefore, the Zn/Mg ratio might not have a notable influence on the macroscopic crack growth rate at room temperature. However, Schwarzenböck et al. found that at 70°C, alloy 7050-T7651 was less sensitive to HEAC than other overaged alloys with a greater Zn/Mg content (7037, 7085 and 7449) [10]. AA7050-T7651 displayed lower stage I and II crack growth rates and a higher K_{IEAC} value. Therefore, the influence of the Zn/Mg ratio may be more significant at higher temperatures.

AA7075 in the -T651 peak aged condition is much more sensitive than the alloys in an overaged condition, with a crack growth rate of 5.1×10^{-6} mm/s (more than an order of magnitude greater). Therefore, the alloy temper seems to have a more serious effect on the

crack growth rate at room temperature than the Zn/Mg ratio. Increased over-ageing has been demonstrated to improve the resistance of 7xxx alloys to HEAC at the expense of strength [29, 30, 31, 32, 33]. However, the influence of over-ageing on the HEAC resistance is dependent on the alloy composition [34].

A previous study from the authors revealed that AA7449-T7651 was much more sensitive than the peak aged AA7075-T651 to the formation of cracks from smooth specimens, despite being in an overaged condition [2]. This was consistent with the safety information bulletin from the EASA [1]. The bulletin informed that aircraft components made from novel alloys (including AA7449) were found to fail from HEAC. The increased susceptibility relative to commonly used alloys, was attributed to the Zn/Mg ratio. These reports are not in accord with the crack growth rates at room temperature shown in this article. The crack growth rate of AA7075-T651 was determined to be more than an order of magnitude greater despite the lower Zn/Mg ratio. It is unclear why there is such a great discrepancy between the time to failure of the 4-point bend samples and the crack growth rates in DCB samples of AA7449-T7651 and AA7075-T651 [2]. It must be noted that the AA7075-T651 alloy presented in Figure 4 [3] is probably not comparable to the alloy used by the authors to perform 4-point bend tests [2]. Additionally, the DCB specimens are pre-cracked and have much larger cracks with a width of 25.4 mm, while smooth specimens must nucleate new cracks that necessarily need to grow from a very low size. Therefore, DCB tests do not account for microstructurally short cracking. Consequently, small barriers to growth (e.g triple junctions) have less impact on the crack growth rates. This was demonstrated by the lifted grains present in the fracture surface (exemplified in Figure 7(a)) and the lack of segmented cracks at high stress intensity factors (Figure 6(c)). As the cracks were much larger, the ligaments produced from crack branching could be ruptured and deformed with more ease than would be possible in microscopic cracks present in smooth specimens [2, 35]. Therefore, the crack growth behaviour can differ considerably with respect to the 4-point bend samples.

For the crack growth rate of stage II cracking, Young and Scully noted that the change in activation energy caused by overaging in AA7050 was similar to the change in activation energy of the diffusion rates [5]. Therefore the rate limiting step during stage II was attributed to the rate of internal hydrogen diffusion. The activation energy for v_{II} of AA7449-T7651 was found to be similar to that of AA7050 (Table 5). Thus, hydrogen diffusion could also be the rate limiting step during stage II. This would be consistent with the observations at room temperature that the peak aged alloy AA7075 was more sensitive than the overaged alloys. Coarser strengthening precipitates from overaging result in irreversible trapping and reduced diffusion rates [23, 27]. Thus, increased ageing may reduce the crack growth rates significantly during stage II. A more systematic approach with greater control of the composition, microstructure and ageing condition of the alloys must be performed to better correlate these variables with K_{IEAC} and v_{II}.

5. Conclusion

This study investigated the influence of temperature on the HEAC crack growth rates of AA7449-T7651 during stage I and II. The results found the following:

1. The threshold stress intensity factor (K_{IEAC}) was found to decrease with increasing temperature. This was likely due to an increase in the hydrogen solubility with temperature (see section 4.1).
2. The stage II crack growth rate of AA7449-T7651 was identified to follow Arrhenius kinetics. The activation energy was estimated as 84.7 kJ/mol at a value of K_I = 14.5 MPa $\sqrt{\text{m}}$. This was similar to peak aged AA7050 from a previous study [5].
3. The crack growth rate of AA7449-T7651 at room temperature is similar to that of AA7075-T7651 and overaged AA7050, despite the differences in composition. However, peak aged AA7075-T651 was found to crack more than an order of magnitude faster. Therefore, it is likely that the stage II crack growth rate at room temperature is more sensitive to the alloy temper than the Zn/Mg ratio.
4. Cracking was to a large extent intergranular. Cracks were found to branch particularly at the interface of recrystallised grains, which diverted the cracks from the main propagation direction.

6. Further work

The data set from this article must be expanded in order to make more definitive conclusions about the influence of temperature on the HEAC behaviour of AA7449-T7651. The authors will therefore aim to cover several open items in a follow-up article, including:

- Performing experiments to assess the influence of HCl gas on the HEAC rate of AA7449 in moist air.

This will involve cracking DCB samples in environments with a varying HCl gas content, with all other variables kept constant (relative humidity and temperature).

- Performing a comparison of the HEAC fracture surfaces of AA7449-T7651 obtained at different temperatures. This will help identifying differences in the cracking behaviour and determine whether the HEAC mechanisms remain the same at lower temperatures.

- The data at room temperature is incomplete, as cracking was negligible at stress intensity factors below 16.7 MPa $\sqrt{\text{m}}$. The authors will therefore carry out repeat runs at room temperature with a higher starting stress intensity factor. This will aim to capture the HEAC behaviour during stages I and II.

7. Appendix A. Supplementary data

Supplementary material related to this article can be found in the online version, at...

8. Declaration of competing interest

The authors declare that they have no known competing financial interests or personal relationships that could have appeared to influence the work reported in this paper.

9. Acknowledgement

I would like to acknowledge the Engineering and Physical Sciences Research Council (EPSRC) for providing funding in a Doctoral Training Partnership (DTP). This funding is provided for a PhD in the University of Bristol (UK). I would also like to acknowledge the support of Alvin Chan and Henry Hall during the experimental design stage.

References

[1] E. A. S. A. (EASA), Environmentally assisted cracking in certain aluminium alloys, https://ad.easa.europa.eu/ad/2018-04R1, 2018.

[2] U. De Francisco, N. O. Larrosa, M. J. Peel, Hydrogen environmentally assisted cracking during static loading of aa7075 and aa7449, Materials Science and Engineering: A 772 (2020) 138662.

[3] M. O. Speidel, M. V. Hyatt, Stress-corrosion cracking of high-strength aluminum alloys, in: Advances in corrosion science and technology, Springer, 1972, pp. 115–335.

[4] M. O. Speidel, Stress corrosion cracking of aluminum alloys, Metallurgical and Materials Transactions A 6 (1975) 631–651.

[5] G. A. Young, J. R. Scully, The effects of test temperature, temper, and alloyed copper on the hydrogen-controlled crack growth rate of an al-zn-mg-(cu) alloy, Metallurgical and Materials Transactions A 33 (2002) 1167–1181.

[6] C. Ferrer, M. Koul, B. Connolly, A. Moran, Improvements in strength and stress corrosion cracking properties in aluminum alloy 7075 via low-temperature retrogression and re-aging heat treatments, Corrosion 59 (2003) 520–528.

[7] S. Knight, K. Pohl, N. Holroyd, N. Birbilis, P. Rometsch, B. Muddle, R. Goswami, S. Lynch, Some effects of alloy composition on stress corrosion cracking in al–zn–mg–cu alloys, Corrosion Science 98 (2015) 50–62.

[8] B. J. Connolly, K. L. Deffenbaugh, A. L. Moran, M. G. Koul, Environmentally assisted crack growth rates of high-strength aluminum alloys, JOM 55 (2003) 49–52.

[9] G. K. Cole, G. Clark, P. Sharp, The Implications of Corrosion with respect to Aircraft Structural Integrity., Technical Report, AERONAUTICAL AND MARITIME RESEARCH LAB MELBOURNE (AUSTRALIA), 1997.

[10] E. Schwarzenböck, E. Ollivier, A. Garner, A. Cassell, T. Hack, Z. Barrett, C. Engel, T. L. Burnett, H. N. Holroyd, J. D. Robson, P. B. Prangnell, Environmental cracking performance of new generation thick plate 7000-t7x series alloys in humid air, Corrosion Science (2020).

[11] A. Association, et al., International alloy designations and chemical composition limits for wrought aluminum and wrought aluminum alloys, Teal Sheets (2009) 1–28.

[12] E. ASTM, G168-17: Standard practice for making and using precracked double beam stress corrosion specimens, West Conshohocken, PA: ASTM Intl (2017).

[13] E. ASTM, E104-02: Standard practice for maintaining constant relative humidity by means of aqueous solutions, West Conshohocken, PA: ASTM Intl (2012).

[14] R. Opila, C. Weschler, R. Schubert, Acidic vapors above saturated salt solutions commonly used for control of humidity, IEEE Transactions on components, hybrids, and manufacturing technology 12 (1989) 114–120.

[15] J. Fritz, C. Fuget, Vapor pressure of aqueous hydrogen chloride solutions, 0° to 50°c., Industrial & Engineering Chemistry Chemical & Engineering Data Series 1 (1956) 10–12.

[16] N. I. of Standards, T. (NIST), Iupac-nist solubility database, version 1.1, nist standard reference database 106, 2015.

[17] N. H. Holroyd, G. Scamans, Crack propagation during sustained-load cracking of al-zn-mg-cu aluminum alloys exposed to moist air or distilled water, Metallurgical and Materials Transactions A 42 (2011) 3979–3998.

[18] A. Andreikiv, V. Panasyuk, V. Kharin, Theoretical aspects of the kinetics of hydrogen embrittlement of metals, Materials Science 14 (1978) 227–244.

[19] S. Ciaraldi, J. Nelson, R. Yeske, E. Pugh, Hydrogen effects in metals, IM Bernstein and AW Thompson (1980) 437–447.

[20] I. M. Robertson, P. Sofronis, A. Nagao, M. Martin, S. Wang, D. Gross, K. Nygren, Hydrogen embrittlement understood, Metallurgical and Materials Transactions A 46 (2015) 2323–2341.

[21] S. Lynch, Mechanistic and fractographic aspects of stress corrosion cracking, Corrosion Reviews 30 (2012) 63–104.

[22] S.-M. Lee, S.-I. Pyun, Y.-G. Chun, A critical evaluation of the stress-corrosion cracking mechanism in high-strength aluminum alloys, Metallurgical Transactions A 22 (1991) 2407–2414.

[23] J. M. A. Pérez, Desarrollo de nuevos tratamientos térmicos para aleaciones avanzadas de interés aeroespacial, UNIVERSIDAD POLITÉNCICA DE MADIRD (2012).

[24] N. Birbilis, R. Buchheit, Electrochemical characteristics of intermetallic phases in aluminum alloys an experimental survey and discussion, Journal of The Electrochemical Society 152 (2005) B140–B151.
[25] J. Scully, G. Young Jr, S. Smith, Hydrogen solubility, diffusion and trapping in high purity aluminum and selected al-base alloys, in: Materials Science Forum, volume 331, Trans Tech Publ, pp. 1583–1600.
[26] E. Martínez-Pañeda, C. F. Niordson, R. P. Gangloff, Strain gradient plasticity-based modeling of hydrogen environment assisted cracking, Acta Materialia 117 (2016) 321–332.
[27] M. S. Bhuiyan, H. Toda, Z. Peng, S. Hang, K. Horikawa, K. Uesugi, A. Takeuchi, N. Sakaguchi, Y. Watanabe, Combined microtomography, thermal desorption spectroscopy, x-ray diffraction study of hydrogen trapping behavior in 7xxx aluminum alloys, Materials Science and Engineering: A 655 (2016) 221–228.
[28] R. P. Wei, Fracture mechanics: Integration of mechanics, materials science and chemistry, Cambridge University Press, 2010.
[29] M. A. Krishnan, V. Raja, Development of high strength aa 7010 aluminum alloy resistant to environmentally assisted cracking, Corrosion Science 109 (2016) 94–100.
[30] W. Qi, R. Song, X. Qi, H. Li, Z. Wang, C. Wang, J. Jin, Hydrogen embrittlement susceptibility and hydrogen-induced additive stress of 7050 aluminum alloy under various aging states, Journal of Materials Engineering and Performance 24 (2015) 3343–3355.
[31] Z. Chen, Y. Mo, Z. Nie, Effect of zn content on the microstructure and properties of super-high strength al-zn-mg-cu alloys, Metallurgical and Materials Transactions A 44 (2013) 3910–3920.
[32] B. Kannan, V. Raja, Hydrogen embrittlement susceptibility of over aged 7010 al-alloy, Journal of materials science 41 (2006) 5495–5499.
[33] D. Nguyen, A. Thompson, I. Bernstein, Microstructural effects on hydrogen embrittlement in a high purity 7075 aluminum alloy, Acta Metallurgica 35 (1987) 2417–2425.
[34] S. Lynch, S. Knight, N. Birbilis, B. Muddle, Stress-corrosion cracking of al-zn-mg-cu alloys effects of composition and heat-treatment, in: Effects of Hydrogen on Materials: Proceedings of the 2008 International Hydrogen Conference, September 7-10, 2008, Jackson Lake Lodge, Grand Teton National Park, Wyoming, USA, ASM International, p. 243.
[35] T. L. Burnett, N. H. Holroyd, G. M. Scamans, X. Zhou, G. E. Thompson, P. J. Withers, The role of crack branching in stress corrosion cracking of aluminium alloys, Corrosion Reviews 33 (2015) 443–454.